iScience

CellPress
OPEN ACCESS

Article

Antifungal mechanisms of silver nanoparticles on mycotoxin producing rice false smut fungus

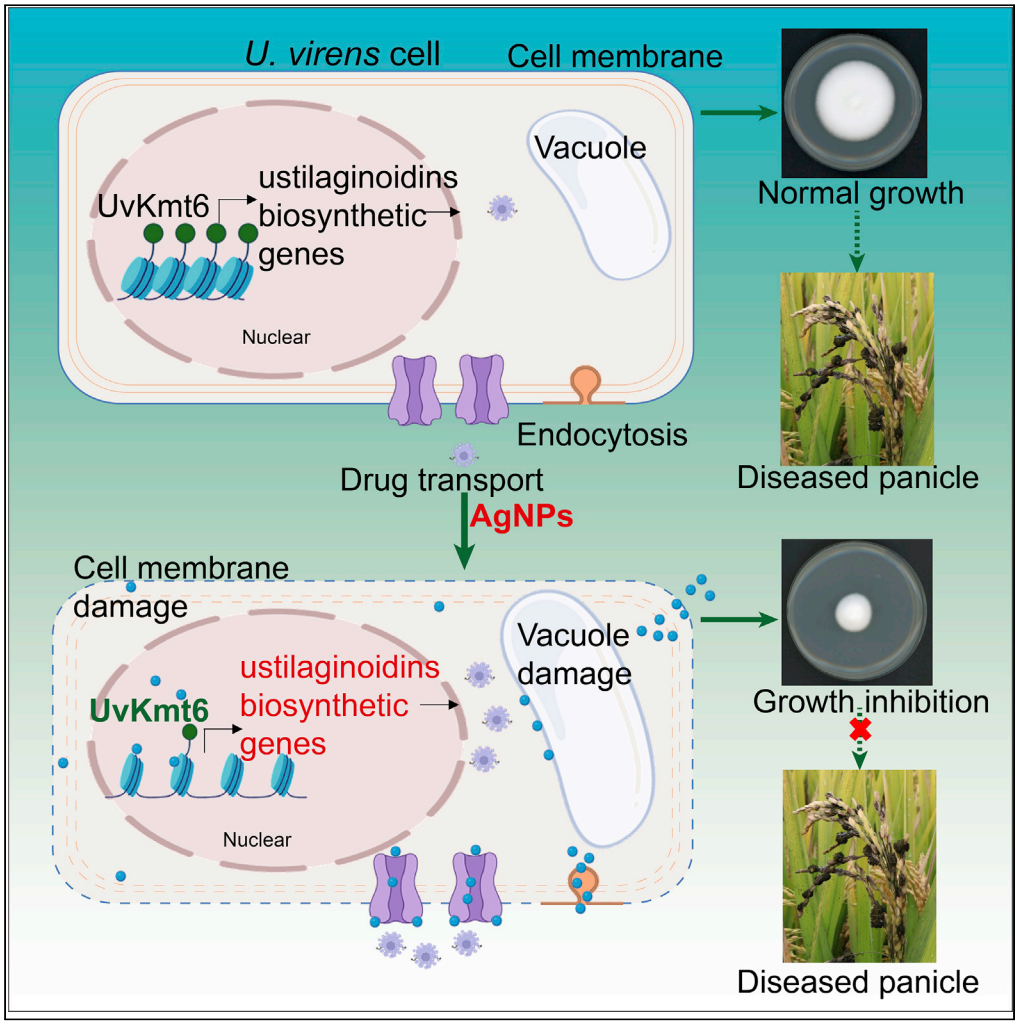

Hui Wen, Huanbin Shi, Nan Jiang, Jiehua Qiu, Fucheng Lin, Yanjun Kou

kouyanjun@caas.cn

Highlights

Inhibition of AgNPs on *Ustilaginoidea virens* growth displayed a concentration-dependent manner

Abnormalities of fungal morphology were observed upon exposure to AgNPs

AgNPs resulted in the up-regulation of ustilaginoidin biosynthetic genes

AgNPs might reduce the UvKmt6-mediated H3K27me3 modification

Wen et al., iScience *26*, 105763
January 20, 2023
https://doi.org/10.1016/j.isci.2022.105763

iScience

CellPress
OPEN ACCESS

Article

Antifungal mechanisms of silver nanoparticles on mycotoxin producing rice false smut fungus

Hui Wen,[1,4] Huanbin Shi,[1,4] Nan Jiang,[1] Jiehua Qiu,[1] Fucheng Lin,[2,3] and Yanjun Kou[1,5,*]

SUMMARY

***Ustilaginoidea virens*, which causes rice false smut disease, is a destructive filamentous fungal pathogen, attracting more attention to search for effective fungicides against *U. virens*. Here, the results showed that the inhibition of 2 nm AgNPs on *U. virens* growth and virulence displayed concentration-dependent manner. Abnormalities of fungal morphology were observed upon exposure to AgNPs. RNA-sequencing (RNA-seq) analysis revealed that AgNPs treatment up-regulated 1185 genes and down-regulated 937 genes, which significantly overlapped with the methyltransferase UvKmt6-regulated genes. Furthermore, we found that AgNPs reduced the UvKmt6-mediated H3K27me3 modification, resulting in the up-regulation of ustilaginoidin biosynthetic genes The decrease of H3K27me3 level was associated with the inhibition of mycelial growth by AgNPs treatment. These results suggested that AgNPs are an effective nano-fungicide for the control of rice false smut disease, but when using AgNPs, it needs to be combined with mycotoxin-reducing fungicides to reduce the risk of toxin pollution.**

INTRODUCTION

In recent years, nanotechnology has attracted more and more attention from researchers because of its wide application in many fields, including agricultural pest and disease control.[1,2] As we all know, nano-fungicides, nano-pesticides, and nano-herbicides have gradually begun to be applied in agricultural practice.[3] In particular, AgNPs are increasingly considered to be useful for the prevention and control of pathogens of crops because micromolar doses of AgNPs are sufficient to kill microbial pathogens.[4] The use of AgNPs, serving as a potential substitute, could be a transformation of fungicide to inhibit plant diseases.[5] Recent study showed that low doses of AgNPs increases the yield and tillering of rice, which provides a positive theoretical basis for the practical application of AgNPs.[6]

Silver is a well-documented antimicrobial agent, which has been proven to kill bacteria, fungi and certain viruses.[7] Nanotechnology provides a new basis for the chemical and physical structural modification of silver, which improves the antimicrobial potential of silver. The physicochemical properties of AgNPs and their interactions with cells are very different from those of silver ions,[8] resulting in differences in their mode of antimicrobial action.[9] Those physicochemical properties include large surface/mass ratio, higher reaction rate, lower toxicity, environmentally friendly, and cost-efficiency. Recently, studies have been carried out widely and confirmed the antimicrobial properties of AgNPs against various pathogens such as *Aspergillus* sp., *Fusarium* sp., *Candida albicans*, *Colletotrichum gloesporioides*, *Staphylococcus* sp. and *Bacillus* sp., as well as against some multidrug resistance microbes.[8,10–13] AgNPs exert antimicrobial activity by various mechanisms, including adhesion on the surface of cell wall and membrane, penetration into cells, disruption of intracellular structures, production of cellular toxicity and oxidative stress and modulating the signaling transduction.[14] At present, studies of AgNPs against the pathogenic fungi of rice are limited, and their molecular mechanisms on pathogenic microbes have not been fully elucidated.

In addition to antifungal activities, relevant studies have also shown the potential of AgNPs in changing fungal secondary metabolism. In the molds *Aspergillus* sp. and *Penicillium chrysogenum*, AgNPs play an inhibitory role in the production of mycotoxin by influencing the biosynthesis of organic acid, oxalic and citric acid.[15] Similarly, in the plant pathogenic filamentous fungus *Aspergillus parasiticus*, engineered

[1]State Key Laboratory of Rice Biology, China National Rice Research Institute, Hangzhou 311400, China

[2]College of Agriculture and Biotechnology, Zhejiang University, Hangzhou 310058, China

[3]State Key Laboratory for Managing Biotic and Chemical Threats to the Quality and Safety of Agro-products, Institute of Plant Protection and Microbiology, Zhejiang Academy of Agricultural Sciences, Hangzhou 310021, China

[4]These authors contributed equally

[5]Lead contact

*Correspondence: kouyanjun@caas.cn

https://doi.org/10.1016/j.isci.2022.105763

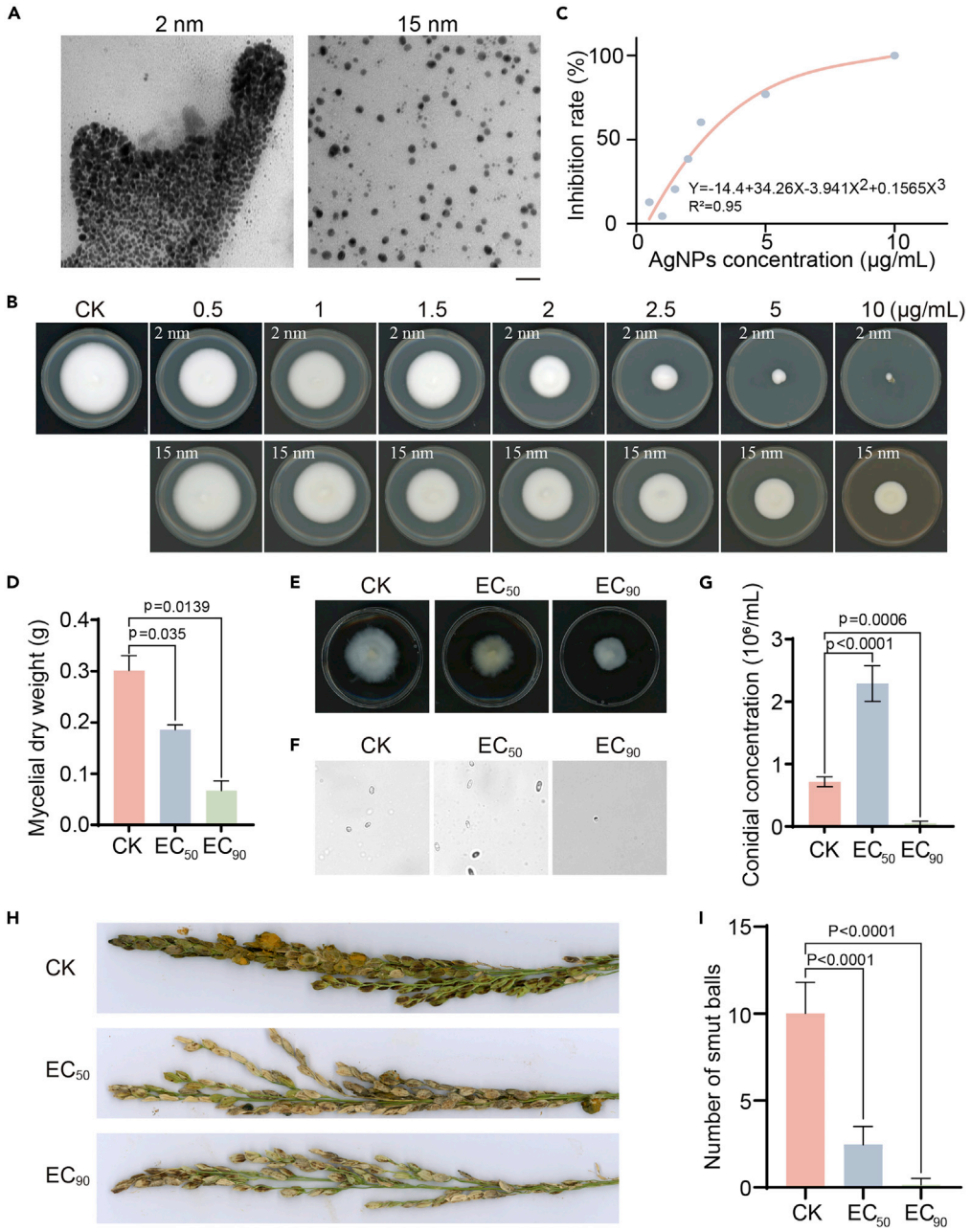

Figure 1. AgNPs affect mycelial growth, conidiation, and virulence of *U. virens*

(A) TEM images of 2 nm and 15 nm AgNPs used in this study. Bar = 100 nm.

(B) AgNPs inhibited the mycelial growth of *U. virens* in a size- and concentration-dependent manner. Mycelial plugs of the wild-type *U. virens* strain HWD were cultured on PSA plates with indicated concentrations of AgNPs for 14 days.

(C) The EC_{50} and EC_{90} were calculated based on the AgNPs concentrations and the relative growth inhibition rates of colonies.

(D) AgNPs treatment inhibited the mycelial growth of *U. virens*. Mycelia cultured with or without 2 nm AgNPs in liquid PS medium for 7 days were collected and weighted after drying.

(E) Morphology of mycelial pellet cultured in the PS medium with or without 2 nm AgNPs.

(F-G) AgNPs treatment affects the conidiation of *U. virens*. Six mycelial plugs were inoculated in the same volume of PS medium without or with 2 nm AgNPs at concentrations equal to EC_{50} and EC_{90}. After 7 days, the conidia were counted using a hemacytometer and converted to the number of conidia per milliliter. The images of conidia were captured using a bright field microscope. Bar = 5 μm.

Figure 1. *Continued*

(H-I) AgNPs treatment reduced the virulence of *U. virens*. The PS medium cultivated-HWD strain was incubated for 1 day with different concentrations of AgNPs to obtain the mixture of hyphae and spores. Each mixture inocula were injected into 10-20 panicles of TP309 cultivar at the booting stage. Rice panicles with smut balls were counted and photographed at 3-weeks post-inoculation. Data shown in (D), (G), and (I) are presented as the means ± SD. p values represent significant difference between CK and AgNPs treatment.

AgNPs inhibit the biosynthesis of aflatoxin. In addition, investigation on the effects of AgNPs on toxigenic *Fusarium* spp. revealed that AgNPs could reduce the secretion of deoxynivalenol (DON) mycotoxins.[8] In contrast, some studies showed that AgNPs treatment induces the transcription of DON synthesis-related genes, formation of toxisome and mycotoxin production by stimulating the generation of reactive oxygen species in *Fusarium graminearum*.[16] Taken together, these studies indicate that the roles of AgNPs in the fungal secondary metabolism are diverse, and the exact mechanisms remain poorly understood.

Ustilaginoidea virens, the causal agent of the rice false smut disease, is a destructive filamentous ascomycete fungal pathogen in rice-growing regions worldwide. The typical symptom caused by *U. virens* is the replacement of seeds with the formation of false smut balls, which initially turn yellow orange to green and finally turns green black.[17] The infection of *U. virens* not only reduces rice production but also threatens food safety due to the contamination of mycotoxins including ustiloxins and ustilaginoidins. Among them, the ustiloxins inhibit the microtubule assembly and skeleton formation of eukaryotic cells.[18] Moreover, ustilaginoidins, a class of bis-naphtho-γ-pyrones, lead to teratogenicity in the development of mouse embryo and midbrain cells, cytotoxic activities, and inhibition the elongation of rice seed radicle.[19] It is worth noting that although there are differences in the incidence of rice false smut disease among rice varieties, most of them are susceptible varieties.[20] Therefore, it is necessary to explore new materials that can possess antifungal effects against *U. virens*.[21] Evidence suggest that AgNPs inhibit a variety of microorganisms and alter the secondary metabolism of fungi.[22,23] However, it is unclear whether AgNPs have antifungal activity against *U. virens* and whether there is a potential risk of using AgNPs to control rice false smut disease.

In this study, we set out to determine the effects of AgNPs on the rice false smut fungus *U. virens* including growth, virulence, fungal morphology, and ultrastructure of cells, and further depicted the molecular mechanism of AgNPs action on *U. virens*. Notably, we found that AgNPs stimulate the up-regulation of ustilaginoidins synthesis-related genes by decreasing the level of H3K27me3 modification in *U. virens*.

RESULTS

Silver nanoparticles inhibit the fungal growth, conidiation, and virulence in *U. virens* in a dose-dependent manner

More and more evidence showed that AgNPs have antimicrobial activity, which is determined by their physical and chemical properties, including particle size and dose.[24–26] AgNPs with 2 nm and 15 nm in diameter were used in this study and observed by SEM (Figure 1A). To analyze the effect of AgNPs on *U. virens*, we evaluated the mycelial growth of the wild-type strain HWD on the PSA plates amended with a series of different concentrations of 2 nm and 15 nm AgNPs, respectively. After 14 days of incubation, we found that the mycelial growth was inhibited by AgNPs with diameters of both 2 and 15 nm (Figure 1B). Quantitative data showed that AgNPs with a diameter of 2 nm displayed stronger antifungal activity than that of 15 nm. In contrast, treatment with water as the control showed no antimicrobial effect in *U. virens*. In addition, dose-dependent response was observed when *U. virens* was exposed to concentrations of AgNPs in the range of 0.5-10 μg/mL. The mycelial growth decreased significantly with the increase in AgNPs concentration (Figure 1B). Furthermore, EC_{50} and EC_{90} values (the effective concentrations to cause inhibitions by 50 and 90%), which are commonly used to show fungicide potency, were determined using a mycelial growth analysis. The EC_{50} and EC_{90} for the 2 nm AgNPs were found to be 2.6 μg/mL and 6.72 μg/mL (Figure 1C), respectively. After treating the seven *U. virens* strains isolated from the field with different concentrations of AgNPs, the results showed that the EC_{50} was in the range of 2.31-2.92 μg/mL (Table S2). Moreover, this mycelial growth inhibition was further confirmed by measuring mycelial dry weight and the sizes of mycelial pellets in the liquid cultures with 2 nm AgNPs at concentrations of EC_{50} and EC_{90}. Consistent with the aforementioned results, AgNPs treatment reduced the mycelial weight and the sizes of mycelial pellets in *U. virens* (Figures 1D and 1E). Collectively, these results indicated that AgNPs play important roles in inhibiting fungal growth in *U. virens*.

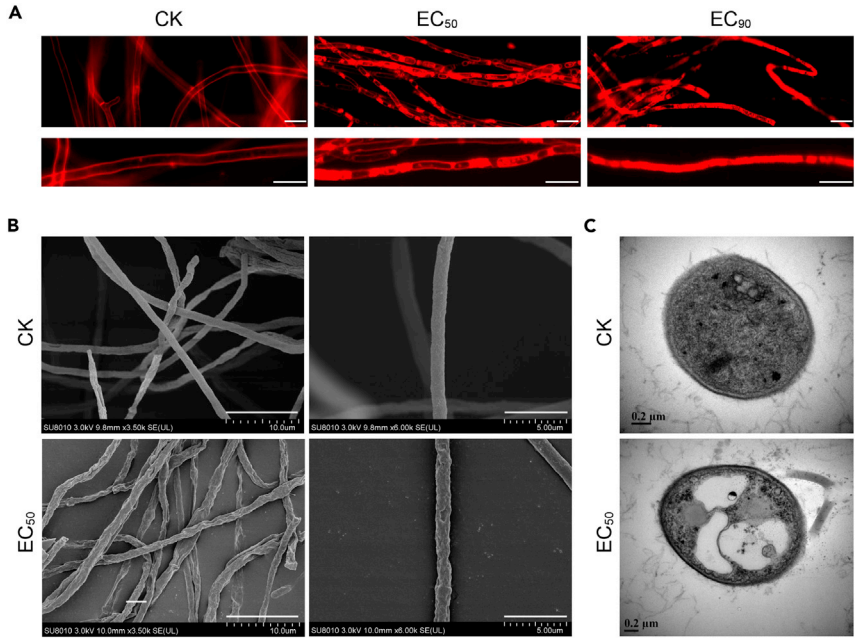

Figure 2. AgNPs treatment disturbs fungal hyphal morphology of *U. virens*

(A) FM4-64 staining of *U. virens* mycelia treated with AgNPs. After mycelia of the wild-type *U. virens* strain were cultured in PS medium for 7 days, 2 nm AgNPs of EC_{50} (2.16 μg/mL) and EC_{90} (5.78 μg/mL) final concentrations were added to the mycelia and then cultured for 24 h. The mycelia were observed and photographed 20 min after FM4-64 staining. Bar = 10 μm. Mycelia treated with AgNPs at a concentration equal to EC_{50} were imaged by scanning electronic microscopy (SEM) (B) and transmission electronic microscopy (TEM) (C). The bar and the length it representation are displayed in each image.

To investigate the role of AgNPs in conidiation, the same amount of mycelial plugs of the wild-type *U.virens* strain HWD were cultured in the liquid PS and PS with 2 nm AgNPs at different concentrations. After being cultured for 7 days, conidiation was evaluated by determining conidial concentration. The results revealed that the conidiation was significantly increased by 2 nm AgNPs at a concentration of EC_{50}, but highly decreased at a concentration of EC_{90} (Figures 1F and 1G). Consistently, microscopic observation further confirmed that conidial germination increased at a concentration of EC_{50} and decreased at a concentration of EC_{90} (Figure S1). These results suggested that AgNPs affect the conidiation of *U. virens* depending on their concentration.

To determine whether AgNPs affect the virulence of *U. virens*, AgNPs were supplemented when the mixture of hyphae and spores was inoculated into rice panicles of the TP309 cultivar. The *U. virens* strain without AgNPs served as a control. The assessment of disease symptoms at 3 weeks post-inoculation showed that the panicles inoculated with 2 nm AgNPs formed fewer smut balls than control, and the number of smut balls decreased with the increase in the concentration of AgNPs (Figures 1H and 1I). These results revealed that 2 nm AgNPs inhibit *U. virens* infection.

Silver nanoparticles disrupt the fungal morphology of *U. virens*

AgNPs are known to have antibacterial and cytotoxic potential because AgNPs are easy to enter into the cells, leading to the destruction of membrane and intracellular organelles and modulation of signal transduction pathways.[27,28] To investigate whether the membrane and vacuolar organelle are affected, the amphiphilic styryl dye FM4-64 staining was performed with mycelia cultured in the PS medium without or with 2 nm AgNPs at concentrations equal to EC_{50} and EC_{90}. FM4-64 is a valuable tool with red fluorescence to monitor intracellular membrane morphologies and dynamics and in particular endocytic pathways. As shown in Figure 2A, without AgNPs treatment, the cell membrane of *U. virens* cells could be stained red by FM4-64. In contrast, the plasma membranes and vacuole membranes of *U. virens* were stained by FM4-64 when mycelia were treated with an EC_{50} final concentration of AgNPs, and the red fluorescence was diffuse in the *U. virens* cells treated with AgNPs at an EC_{90} concentration (Figure 2A). In

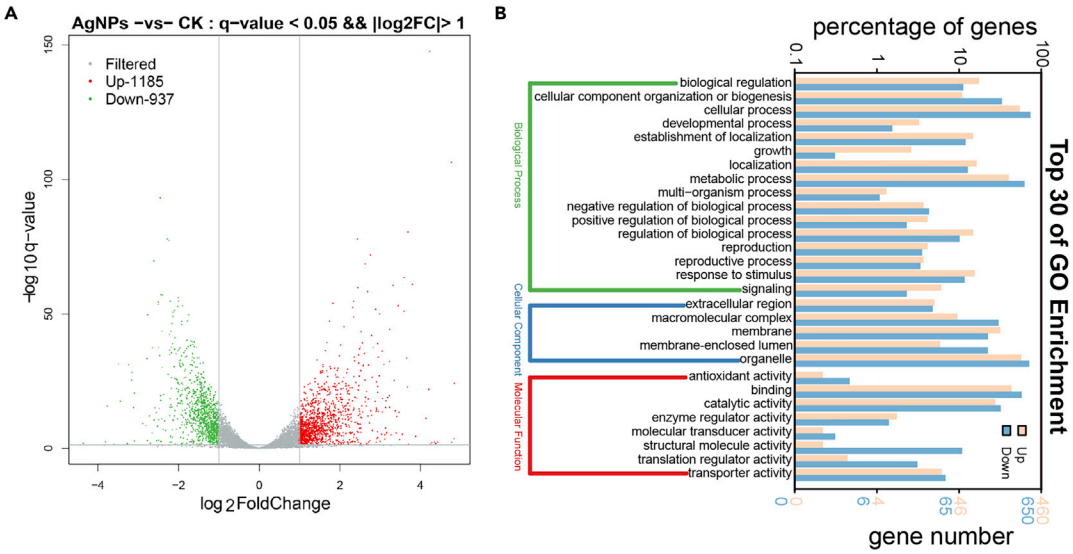
A
AgNPs −vs− CK : q−value < 0.05 && |log2FC|> 1
Filtered
Up-1185
Down-937
−log10 q−value
log2FoldChange
B
percentage of genes
biological regulation
cellular component organization or biogenesis
cellular process
developmental process
establishment of localization
growth
localization
metabolic process
multi−organism process
negative regulation of biological process
positive regulation of biological process
regulation of biological process
reproduction
reproductive process
response to stimulus
signaling
extracellular region
macromolecular complex
membrane
membrane-enclosed lumen
organelle
antioxidant activity
binding
catalytic activity
enzyme regulator activity
molecular transducer activity
structural molecule activity
translation regulator activity
transporter activity
Biological Process
Cellular Component
Molecular Function
Up
Down
Top 30 of GO Enrichment
gene number

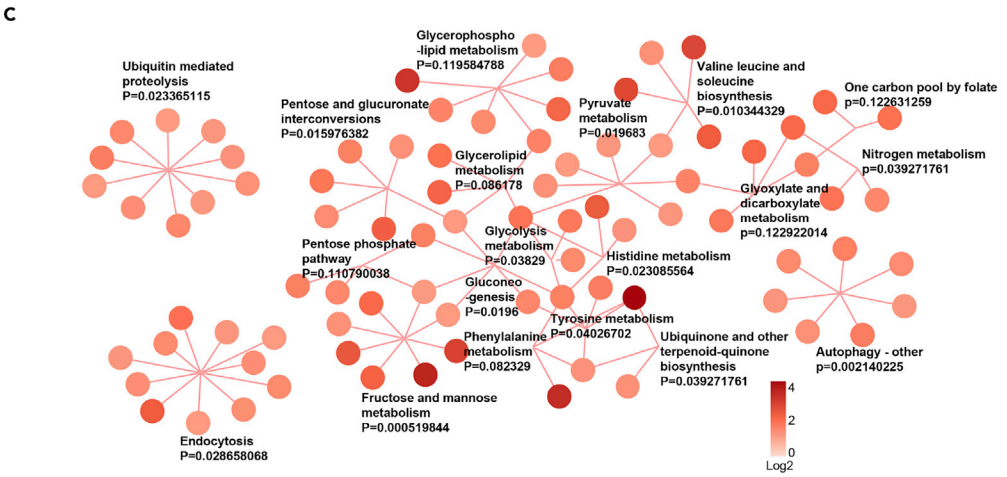
C
Ubiquitin mediated proteolysis P=0.023365115
Glycerophospho -lipid metabolism P=0.119584788
Pentose and glucuronate interconversions P=0.015976382
Pyruvate metabolism P=0.019683
Valine leucine and soleucine biosynthesis P=0.010344329
One carbon pool by folate p=0.122631259
Nitrogen metabolism p=0.039271761
Glycerolipid metabolism P=0.086178
Glyoxylate and dicarboxylate metabolism p=0.122922014
Pentose phosphate pathway P=0.110790038
Glycolysis metabolism P=0.03829
Histidine metabolism P=0.023085564
Gluconeo -genesis P=0.0196
Tyrosine metabolism P=0.04026702
Phenylalanine metabolism P=0.082329
Ubiquinone and other terpenoid-quinone biosynthesis P=0.039271761
Autophagy - other p=0.002140225
Fructose and mannose metabolism P=0.000519844
Endocytosis P=0.028658068
Log2

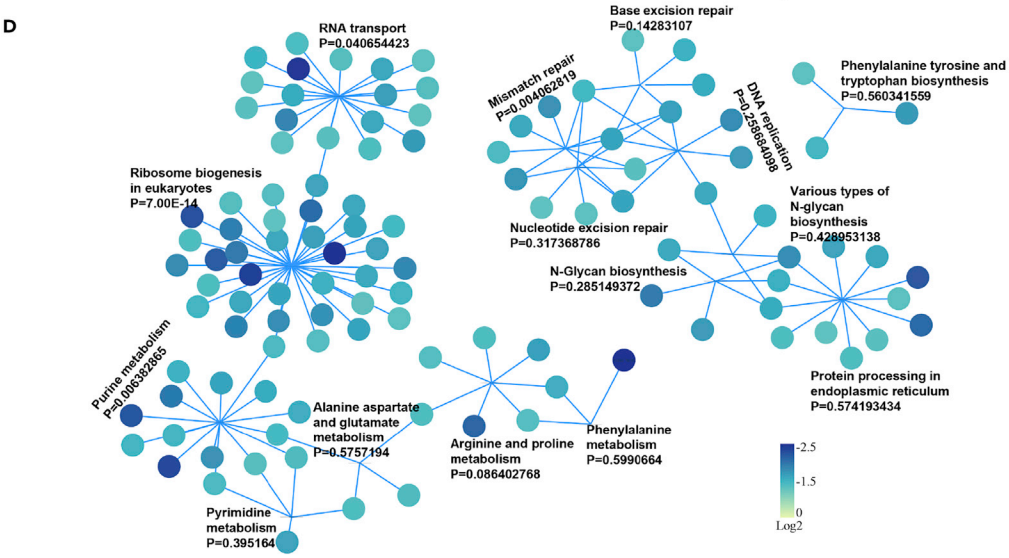
D
RNA transport P=0.040654423
Base excision repair P=0.14283107
Mismatch repair P=0.004062819
DNA replication P=0.258684098
Phenylalanine tyrosine and tryptophan biosynthesis P=0.560341559
Ribosome biogenesis in eukaryotes P=7.00E-14
Nucleotide excision repair P=0.317368786
Various types of N-glycan biosynthesis P=0.428953138
N-Glycan biosynthesis P=0.285149372
Purine metabolism P=0.00638265
Alanine aspartate and glutamate metabolism P=0.5757194
Arginine and proline metabolism P=0.086402768
Phenylalanine metabolism P=0.5990664
Protein processing in endoplasmic reticulum P=0.574193434
Pyrimidine metabolism P=0.395164
Log2

Figure 3. RNA-seq analysis revealed the effects of AgNPs treatment on the transcription of *U. virens*

(A) DEGs of AgNPs treatment with the EC_{50} final concentration are displayed by volcano map. The abscissa shows the fold-changes of up-regulated or down-regulated DEGs, the ordinate displays the level of statistical significance, and the change in gene expression is represented by the q value. Each dot represents a gene, with red dots indicating the up-regulated genes, green dots representing the down-regulated genes, and gray dots denoting the gene without differences.

(B) GO enrichment of DEGs in the comparison of AgNPs treatment and control in *U. virens*. The lower coordinate represents the number of genes enriched in each function, and the upper coordinate represents the percentage of genes enriched in each function among all DEGs. Navajo white and blue represent up-regulated and down-regulated genes, respectively. KEGG network analyses of up-regulated genes (C) and down-regulated genes (D) in AgNPs treated mycelia of *U. virens*. Each circle indicates a corresponding gene. Straight lines emanating from the same center of the circle represent the different genes enriched in this pathway. The color of each circle represents the fold changes in gene expression. RNA-seq analyses were performed with three independent biological replicates.

general, the AgNPs treatment significantly accelerated the FM4-64 staining rate of *U. virens* cells, indicating that cell membranes of the hyphae have been damaged by AgNPs to varying degrees.

To further understand how AgNPs interact with fungal cells, the ultrastructural structures of *U. virens* cells were determined using SEM and TEM analyses. The mycelia of wild-type *U. virens* strain HWD were incubated in the PS medium with or without 2 nm AgNPs at a concentration equal to EC_{50} for SEM observation. SEM images showed that AgNPs treatment resulted in twisted and aberrant hyphae in *U. virens* (Figure 2B). Moreover, craters could be seen on the cell walls when AgNPs were present. These phenomena implied that the AgNPs treatment led to defects in the cell wall of *U. virens*. SEM analyses only revealed the external morphological changes, so it is necessary to further observe internal changes using TEM. As shown in Figure 2C, the structural damages of AgNPs treated *U. virens* cells were clearly visible, including the accumulation of vacuoles or vesicles in the cytoplasm, which is consistent with the results of FM4-64 staining assay (Figure 2A). In conclusion, SEM and TEM observations revealed that both the surface and intracellular organelles of fungal cells were disrupted by AgNPs, resulting in AgNPs being toxic to *U. virens*.

Silver nanoparticles affect the expression of genes related to various metabolic processes in *U. virens*

The modulation of microbial intracellular signaling pathways has been recognized as one of the prominent modes of antimicrobial action of AgNPs.[15,29] To investigate the AgNPs-modulated intracellular signaling pathways, RNA-seq analysis was performed using mycelia of the wild-type *U. virens* strain HWD cultured in the liquid PS medium containing 2 nm AgNPs (EC_{50} concentration) or without AgNPs for 7 days. Compared with the control, a total of 2122 genes were differentially expressed in the AgNPs treated mycelia (adjusted p value <0.05), with 1185 genes up-regulated ($\log_2 > 1$) and 937 down-regulated ($\log_2 < -1$) (Figure 3A). Next, to have a more comprehensive and adequate understanding of the functional classification of DEGs, GO analyses were conducted. The enriched GO classifications of all $p < 0.05$ processes were assigned to three categories: biological process including metabolic process (591 genes), cellular component including genes associated with membrane and organelle (726 genes), and molecular function including catalytic activity (333 genes) (Figure 3B). Overall, the AgNPs-regulated genes were mainly correlated with metabolic process, organelle, and catalytic activity.

Functional KEGG analysis of the up-regulated genes revealed that AgNPs led to the up-regulation of genes related to several metabolism pathways and autophagy. Metabolism pathways, including lipid metabolism and carbohydrate pathways, were likely elevated by AgNPs treatment (Figure 3C). Autophagy is a self-eating process that proteins or organelles within cells are constantly degraded to maintain homeostasis.[30] It is reported that autophagy is positively correlated with lipid metabolism in fungi.[31] In this study, we found that in response to the AgNPs treatment, autophagy was elevated and corresponding lipid metabolisms were enhanced to maintain energy hemostasis within cells. In conclusion, these data suggested that AgNPs may increase the activity of intracellular energy utilization and metabolic processes in *U. virens*.

Functional KEGG analysis of the down-regulated genes revealed that AgNPs treatment may reduce the metabolism of multiple amino acids, including purine, pyrimidine, arginine, proline, alanine, aspartate, and glutamate. Moreover, genes related to several repair processes such as base excision repair, nucleotide excision repair, nucleotide excision, and mismatch repair were also down-regulated by AgNPs. In addition, genes required for the ribosome, phenylalanine, tyrosine and tryptophan biosynthesis and protein processing in the ER were present in AgNPs down-regulated genes (Figure 3D). The basal metabolism and repair processes were significantly disrupted in the hyphae with AgNPs treatment, suggesting that

Figure 4. AgNPs-regulated genes show an overlapping with the genes in the Δ*Uvkmt6* mutant

(A) The overlapping between the DEGs in the Δ*Uvkmt6* mutant versus wild-type and the AgNPs treatment versus control was present in venn diagrams. The two sets' association significance was calculated by TBtools with p value labeled.

(B) GO enrichment analysis of the overlapped DEGs. Only the top 20 are shown. The lower coordinate represents the percentage of genes enriched in each function among all overlapping genes. The number of genes and the p values are marked on each column of the enrichment function.

(C) KEGG enrichment analysis of overlapping DEGs in the Δ*Uvkmt6* mutant versus wild-type and the AgNPs treatment versus control. KEGG enrichment levels were assessed by q-values and the rich factors. The horizontal direction represents Rich factor, which is the ratio of genes in each item. The size of the dot denotes the number of genes enriched in the items, and the color of the dot corresponds to the q value ($q \geq 0.05$). RNA-seq analyses were performed with three independent biological replicates.

AgNPs treatment may result in increased energy expenditure, but reduces the replenishment in hyphae, thus inhibiting the fungal growth in *U. virens*. Taken together, these results revealed that intracellular metabolic processes may be severely affected by AgNPs treatment in *U. virens*.

Silver nanoparticles may be involved in transcriptional regulation partially dependent on the methyltransferase UvKmt6

In our previous study, we found that methyltransferase UvKmt6-mediated H3K27 trimethylation participates in the genome-wide transcriptional repression in *U. virens*.[32] Disruption of *UvKmt6* resulted in reduced growth, conidiation, production in the toxic compounds and/or metabolites in *U. virens*, which are similar to the phenotypes with AgNPs treatment.[32] By comparing the RNA-seq data, we found that the 339 out of 1042 DEGs in the Δ*Uvkmt6* mutant versus wild-type overlapped with 2122 DEGs identified from the AgNPs treatment versus control (Figures 4A and S2). To explore the functional classification of the common DEGs, a GO enrichment analysis was performed. The results showed that the common DEGs in the Δ*Uvkmt6* mutant versus wild-type and the AgNPs treatment versus control were mainly involved in the cell wall structure assembly, transport, metabolism process, and protein unfold (Figure 4B), suggesting that the deletion of *UvKMT6* and AgNPs treatment change the cellular structural integrity in *U. virens*. Furthermore, a KEGG pathway enrichment analysis was carried out to reveal the complex biological behaviors of

the 339 overlapped DEGs. The results showed that the pathways with the greatest number of enrichments were the metabolic pathways, including tyrosine, phenylalanine, arginine, proline, glycerophospholipid, ubiquinone, drug, cytochrome P450, starch, sucrose, methane, retinol and glutathione metabolisms (Figure 4C), indicating that multiple basal protein metabolic pathways are affected by the deletion of *UvKMT6* gene and AgNPs treatment. In conclusion, these results suggested that a part of DEGs from the AgNPs treatment versus control may be associated with the absence of UvKmt6-mediated H3K27me3 occupancy in *U. virens*.

Silver nanoparticles promote the production of toxic compounds as the disruption of *UvKMT6* in *U. virens*

U. virens not only reduces yield by occupying rice grains but also produces toxic compounds, such as ustilaginoidins O, E, F, R2, U, B and I, which inhibit rice seeds germination.[19,33] In *U. virens*, the syntheses of ustilaginoidins require ustilaginoidin biosynthetic genes, such as *ugsZ*, *ugsT*, *ugsO*, *ugsJ*, *ugsL*, *ugsR2* and other genes. When we compared the DEGs in the Δ*Uvkmt6* mutant versus wild-type and the AgNPs treatment versus control, we noticed that ustilaginoidin biosynthetic genes were significantly up-regulated in the AgNPs treatment and the Δ*Uvkmt6* mutant strain (Figures 5A and 5B). To verify RNA-seq results of ustilaginoidin biosynthetic genes, qRT-PCR assays were carried out. Consistent with RNA-seq data, exposure to AgNPs resulted in more than 2-folds up-regulation of ustilaginoidin biosynthetic genes, including *UV8b_2082*, *ugsO*, *UV8b_2084*, *ugsZ*, *ugsT* and *ugsJ* (Figure 5C). The transcription levels of ustilaginoidin biosynthetic genes up-regulated by AgNPs may lead to an increase in the production of toxic compounds, which could be determined via a germination assay of rice seeds in *U. virens*.[33] To test this possibility, the inhibition of cultural filtrates obtained from PS medium with different concentrations of 2 nm AgNPs of 7-days-old wild-type HWD on rice seed germination was evaluated. As shown in Figures 5D and 5E, the shoots of the rice treated by the cultural filtrates with AgNPs were significantly shorter than those of the control, indicating that AgNPs promote the production of toxic compounds which inhibit the growth of shoot during rice seed germination. These results suggested that AgNPs up-regulate the biosynthetic genes of toxic compounds as the disruption of *UvKMT6*, resulting in the increase of toxic compounds production in *U. virens*.

Silver nanoparticles may repress UvKmt6-mediated H3K27me3 modification

Several DEGs, including toxic compounds biosynthetic genes, were found in the Δ*Uvkmt6* mutant versus wild-type and the AgNPs treatment versus control, indicating that the level of UvKmt6-mediated H3K27me3 modification might be changed upon AgNPs treatment. To test this hypothesis, the nucleic proteins of wild-type HWD cultured in the PS medium with or without AgNPs and the Δ*Uvkmt6*-16 mutant were extracted and subjected to immunoblot with the specific H3K27me3 antibody. The immunoblotting results showed that in the Δ*Uvkmt6* mutant, the H3K27me3 modification was almost undetectable compared to obvious band in the wild-type strain (Figure 6A). Moreover, the level of H3K27me3 modification showed a slightly decrease in the wild-type strain upon AgNPs treatment (Figures 6A and S3). These results indicated that AgNPs treatment may reduce the level of UvKmt6-mediated H3K27me3 modification in *U. virens*.

To investigate the response of *U. virens* to AgNPs after knockout of *UvKMT6* gene, mycelial plugs of the wild-type HWD, Δ*Uvkmt6*-16, Δ*Uvkmt6*-18, and Δ*Uvkmt6* complemented strains were inoculated on the PSA plates with or without 2 nm AgNPs, respectively. As shown in Figures 6B and 6C, disruption of *UvKMT6* increased the inhibition rate of AgNPs on the *U.virens*. This result suggested that upon AgNPs treatment, the decrease of UvKmt6-mediated H3K27me3 is associated with the inhibition of mycelial growth.

DISCUSSION

With the development of agriculture, "green technologies" have attracted more and more attention, which is attributed to their high efficiency, non-toxicity, and environmental protection. The rapid development of nanotechnology and widely application of nanomaterials promote us to investigate the application potential of nanoparticles in preventing the rice false smut fungus *U. virens*, an important threat to rice production and quality.[17,34–37] Recent research showed that the application of AgNPs has a low risk of transfer to humans through the food chain. After nanosilver treatment, Ag accumulated in rice tissues including rice seeds. However, Ag was primarily distributed in the rice hull and surface of the grains (bran), and is not

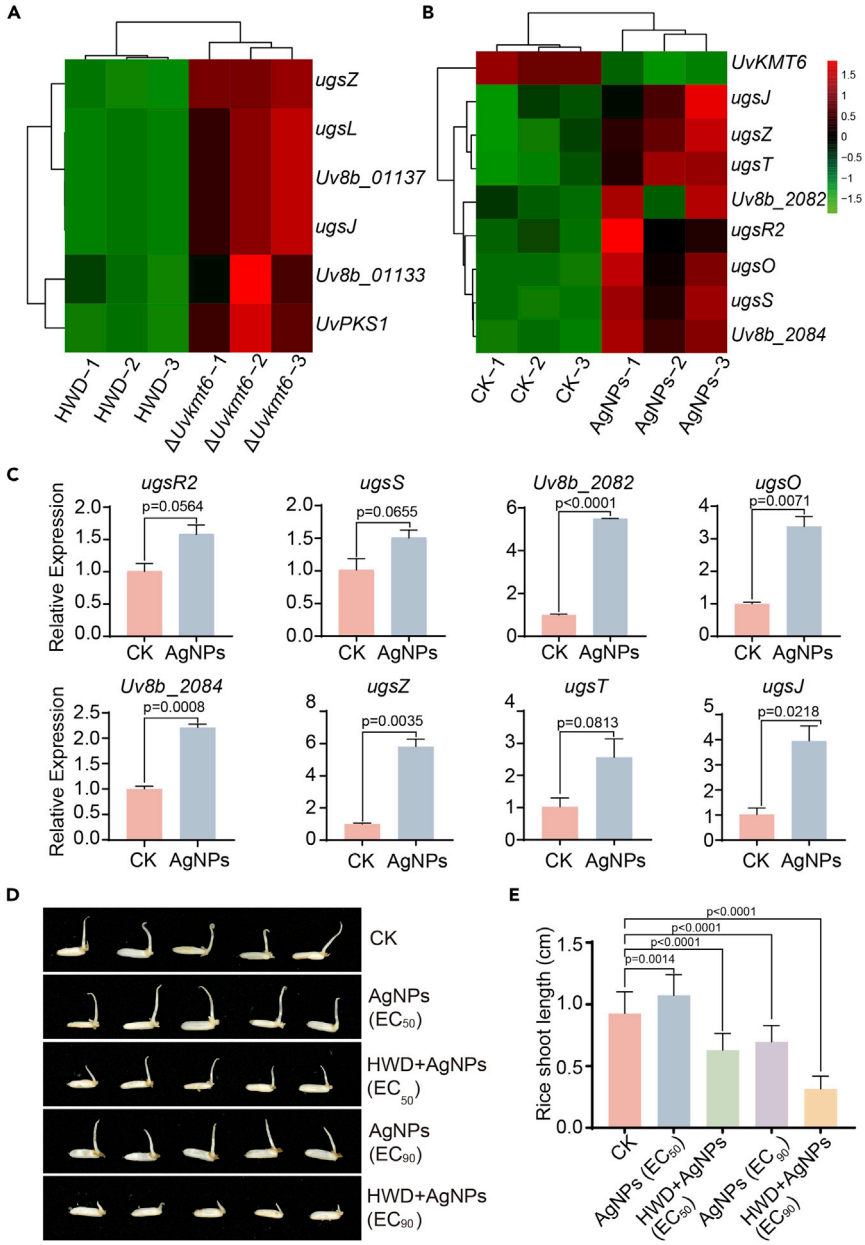

Figure 5. AgNPs activate the transcription of genes related to ustilaginoidins synthesis as the disruption of the *UvKmt6* gene in *U. virens*

(A) Heatmap shows the expression dynamics of ustilaginoidins synthesis-related genes in the Δ*Uvkmt6* compared with those in the wild-type HWD. Every colored cell on the image corresponds to the value of gene expression level, which was detected by RNA-seq and normalized by the *Z* score.

(B) Heatmap shows the transcription dynamics of ustilaginoidins synthesis-related genes in AgNPs treated mycelia compared with control.

(C) The relative expression levels of eight ustilaginoidins synthesis-related genes were verification by qRT-PCR analyses. p values representing significant difference were labeled.

(D-E) The inhibition effects of the cultural filtrates of *U. virens* cultures without or with 2 nm AgNPs at a concentration equal to EC_{50}. Rice seeds were immersed in the cultural filtrates for 7 days and their germinations were determined. Seeds treated with the filtrate of WT strain were used as the control (CK). These experiments were repeated three times with more than 50 seeds each time. p values were generated using the Student's t-test. Data shown in (C) and (E) are presented as the means ± SD. p values represent significant difference between CK and AgNPs treatment.

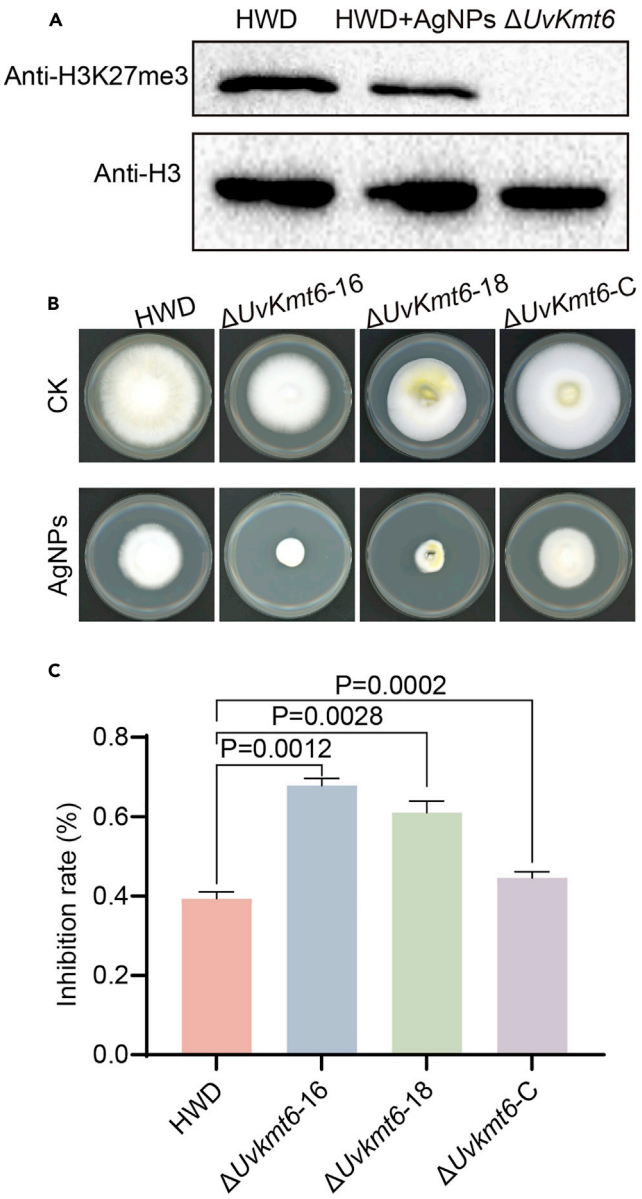

Figure 6. UvKmt6-mediated H3K27me3 modification is involved in the response of *U. virens* to AgNPs treatment

(A) The level of H3K27me3 modification in mycelia of *U. virens* treated with 2 nm AgNPs at a concentration equal to EC_{50} was detected using immunoblotting. The deletion mutant Δ*Uvkmt6* served as a negative control.

(B) Disruption of *UvKMT6* resulted in the decreased sensitivity to AgNPs. Mycelial plugs of the WT, Δ*Uvkmt6*-16, Δ*Uvkmt6*-18, and complemented strain Δ*Uvkmt6*-C were inoculated on PSA plates amended with 2 nm AgNPs at the concentration of EC_{50} for 14 days.

(C) The relative growth inhibition rates of the WT, Δ*Uvkmt6*-16, Δ*Uvkmt6*-18 and complemented strain Δ*Uvkmt6*-C were determined by measuring the diameter of the colonies. Data shown in (C) are presented as the means ± SD. p values represent significant difference between HWD and UvKMT6 strains.

delivered into the polished grains at the 1 mg/kg and 10 mg/kg doses.[6] Due to antimicrobial activities of AgNPs, it is necessary to evaluate the application potential of AgNPs on preventing the phytopathogenic fungi *U. virens*. In this study, we found that AgNPs play inhibitory roles in the growth, conidial development and virulence of *U. virens*. Further studies revealed that AgNPs are involved in the transcriptional regulation of secondary metabolic processes including the production of mycotoxins, which might be through an epigenetic factor UvKmt6-mediated transcriptional repression in *U. virens*.

Several recent studies have shown that AgNPs cause damage to the cell walls of various fungi, such as *C. albicans*[10] and *Trichosporon asahii*.[38] Similarly, the investigation of effects of AgNPs on the wheat scab pathogen *F. graminearum* revealed that hyphal morphology, including cell membrane and cell wall, was disrupted upon AgNPs treatment.[39] This study found that AgNPs inhibit the mycelial growth of *U. virens* in a size-dependent manner. Those results are supported by the fact that smaller diameter nanoparticles have a superior surface area and are easy to penetrate cell walls and membranes to induce intracellular organelles responses.[27] Furthermore, the observations using the TEM, SEM, and FM4-64 staining revealed that the integrity of the cell wall was destroyed and the permeability of the cell membrane was increased by AgNPs treatment (Figures 2A, 2B and 2C). In addition, the results of the RNA-Seq analysis demonstrated that there is a significant change in the expression of the cell membrane and ion transport-related pathway genes after AgNPs treatment (Figure 4B). It is possible that small-grained AgNPs do not only destroy the cell membrane but also are uptaken into the cell by endocytosis to disrupt the intracellular organelles and protein functions, resulting in changes in fungal morphology and various metabolic and signaling pathways.[40] Based on our results, we concluded that the growth inhibition of *U. virens* by AgNPs may be caused by affecting the integrity of fungal cell wall and cell membrane, interrupting the intracellular structures and changing the genome-wide transcription.

Several studies have shown that the area or number of vacuoles is increased after nanomaterial treatment.[41–44] This phenomenon may be caused by an increased level of intracellular autophagy, which is also known as a response against unfavorable factors.[45–47] Consistent with these studies, we also observed an increase in the area of vacuole in the hyphae of *U.virens* after AgNPs treatment (Figure 2C). In addition, RNA-seq data showed that the expression levels of autophagy-related genes were significantly up-regulated. These data implicated the role of autophagy in *U. virens* responding to AgNPs treatment.

Furthermore, nanoparticles and nanomaterials have also been reported to alter the epigenetic modulations in eukaryotic cells.[48–50] The effects of nanomaterials and nanoparticles on epigenetic modifications, including DNA methylation and histone modification, have been found in mammalian cells. For instance, upon 20 nm AuNPs treatment *in vitro*, H3K27me3 levels decreased in small airway epithelial cells.[51] In bladder cancer T24 cells, the methylation of histone H3K27me3 was reduced by a low concentration of zinc oxide nanoparticles,[52] and the descent in EZH2 level was caused by the decrease of H3K27me3 level after human serum nanomaterials treatment.[53] In addition, when mouse erythroleukemia cells were treated with 8 μg/mL AgNPs for 72 h *in vitro*, the global histone modifications H3K4me3 and H3K79me1 were decreased. However, the role of epigenetic modifications in the response of fungi to nanoparticles remains relatively unexplored. This study found that AgNPs treatment reduced the level of UvKmt6-mediated H3K27me3 modification in *U. virens* (Figure 6A). It was known that *UvKMT6* participates in the transcriptional repressions of genes encoding effectors, genes associated with secondary metabolites production, oxidative, osmotic, cell wall, and nutrient starvation stresses response-related genes.[32] Consistent with the reduction of UvKmt6-mediated H3K27me3 modification by AgNPs, the results from RNA-seq analysis demonstrated that the expression levels of effector genes and genes associated with cell wall assembly and secondary metabolites production were regulated by the AgNPs treatment (Figures 4B, 4C and Table S3). In conclusion, these results suggested that AgNP treatment may reprogram the genome-wide transcription partly by changing the level of UvKmt6-mediated H3K27me3 modification in *U. virens*.

There are increasing evidence that the application of nanoparticles can induce the production of mycotoxins. For instance, SiO_2 nanoparticles treatment induces oxidative stress in *Penicillium verrucosum* cells, resulting in the increased production of citrinin, which is a mycotoxin.[54] In *Fusarium* spp., it is reported that AgNPs increase the biogenesis of mycotoxin deoxynivalenol but decrease its secretion.[8] Although AgNPs have been reported to affect the secondary metabolism of fungi, the exact mechanism is not clear. Here, we found that AgNPs treatment reduces the level of UvKmt6-mediated H3K27me3 modification, which regulates the production of mycotoxins in *U. virens*.[32] This conclusion was supported by the results of RNA-seq analyses and qRT-PCR assay, in which ustilaginoidin biosynthetic genes were up-regulated by the AgNPs treatment and disruption of *UvKMT6* gene. In addition, the deletion of *UvKMT6* resulted in reduced sensitivity to AgNPs, suggesting that UvKmt6 is involved in the response to AgNPs in *U. virens*. All these evidence indicated that AgNPs may affect the expression of ustilaginoidin biosynthetic genes by targeting UvKmt6, leading to the increase the ustilaginoidins production in *U. virens*.

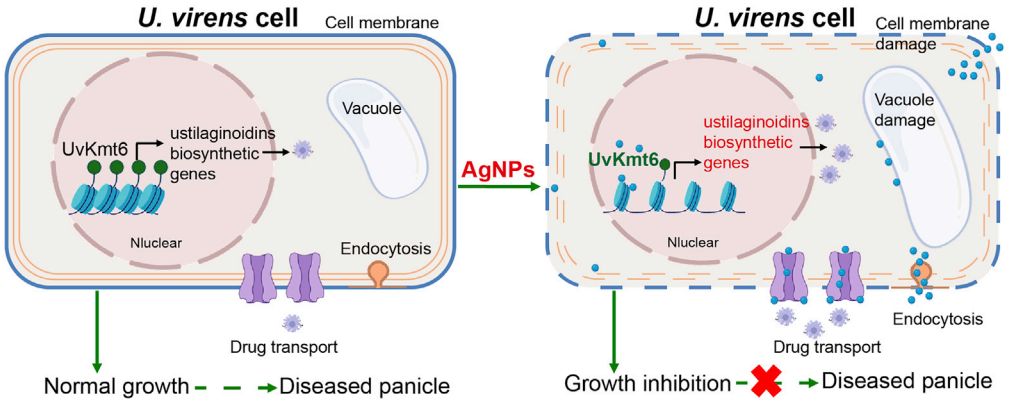

Figure 7. Proposed model shows the antifungal mechanism of AgNPs acting on *U.virens*

Under natural conditions, the normal growth and infection of *U.virens* cause rice false smut on rice panicles. When treated with AgNPs, cell membrane and cell wall are damaged, leading to cell permeability increase and thereby inhibiting the growth and the virulence of *U.virens*. In addition, AgNPs increased the mycotoxins synthesis by influencing methyltransferase UvKmt6-mediated transcriptional repression on ustilaginoidins biosynthetic genes.

Conclusion

To summarize, this study is the first report demonstrating the detailed mechanism of AgNPs against the rice fungal pathogen *U. virens*, providing a theoretical basis for the application of silver nanoparticles in fungal prevention. The results showed that AgNPs affect the integrity of the fungal cell wall and cell membrane, interrupt the intracellular structures, and change genome-wide transcription to inhibit the growth of *U. virens*. However, AgNPs promote the production of toxic compounds by repressing UvKmt6-mediated H3K27me3 modification, suggesting that combinations of AgNPs with mycotoxin-reducing fungicides can be used to control rice false smut disease (Figure 7). These results are helpful to understand the application and concerns of AgNPs in plant fungal disease control.

Limitations of the study

In this study, we suggested that AgNPs reduced the UvKmt6-mediated H3K27me3 modification, resulting in the up-regulation of ustilaginoidin biosynthetic genes and increased the production of toxic compounds. However, it is now apparent that the increased toxin production by the *U. virens* after AgNPs treatment, which will become a major barrier in the future application of AgNPs. As we discussed above, AgNPs need to be combined with mycotoxin-reducing fungicides to reduce the risk of toxin pollution. Therefore, future studies will be essential to illustrate the impacts of combined application on the ability to control *U. virens* and produce toxins.

STAR★METHODS

Detailed methods are provided in the online version of this paper and include the following:

- KEY RESOURCES TABLE
- RESOURCE AVAILABILITY
  - Lead contact
  - Materials availability
  - Data and code availability
- EXPERIMENTAL MODEL AND SUBJECT DETAILS
  - Strains and growth inhibition determination
- METHOD DETAILS
  - Infection assay of *U. virens*
  - Scanning electron microscope (SEM) and transmission electron microscopy (TEM) observations
  - FM4-64 staining and imaging
  - RNA-seq and bioinformatics analyses
  - Quantitative real-time PCR (qRT-PCR) analysis
  - Toxicity assays
  - Detection of H3K27me3 via immunoblotting
- QUANTIFICATION AND STATISTICAL ANALYSIS

SUPPLEMENTAL INFORMATION

Supplemental information can be found online at https://doi.org/10.1016/j.isci.2022.105763.

ACKNOWLEDGMENTS

This research was supported by grants from the National Natural Science Foundation of China (32171944 to YK, 32100161 to JQ), key R&D project of China National Rice Research Institute, grand number "CNRRI-2020-04." This project was also supported by the Chinese Academy of Agricultural Sciences under the "Elite Youth" Program and the Agricultural Sciences and Technologies Innovation Program.

AUTHOR CONTRIBUTIONS

Y. K. designed the experiments. H. W. and H. S. performed most of experiments and analyzed the data. Other authors assisted in experiments and discussed the results. H. W., H. S., and Y. K. wrote the article.

DECLARATION OF INTERESTS

The authors declare no competing interests.

Received: July 25, 2022
Revised: November 3, 2022
Accepted: December 5, 2022
Published: January 20, 2023

REFERENCES

1. Rizwan, M., Ali, S., Zia Ur Rehman, M., Adrees, M., Arshad, M., Qayyum, M.F., Ali, L., Hussain, A., Chatha, S.A.S., and Imran, M. (2019). Alleviation of cadmium accumulation in maize (*Zea mays* L.) by foliar spray of zinc oxide nanoparticles and biochar to contaminated soil. Environ. Pollut. *248*, 358–367. https://doi.org/10.1016/j.envpol.2019.02.031.

2. Chen, F., Bashir, A., Zia Ur Rehman, M., Adrees, M., Qayyum, M.F., Ma, J., Rizwan, M., and Ali, S. (2022). Combined effects of green manure and zinc oxide nanoparticles on cadmium uptake by wheat (*Triticum aestivum* L.). Chemosphere *298*, 134348. https://doi.org/10.1016/j.chemosphere.2022.134348.

3. Goswami, P., Yadav, S., and Mathur, J. (2019). Positive and negative effects of nanoparticles on plants and their applications in agriculture. Plant Sci. Today *6*, 232–242. https://doi.org/10.14719/pst.2019.6.2.502.

4. Guilger-Casagrande, M., Germano-Costa, T., Bilesky-José, N., Pasquoto-Stigliani, T., Carvalho, L., Fraceto, L.F., and de Lima, R. (2021). Influence of the capping of biogenic silver nanoparticles on their toxicity and mechanism of action towards *Sclerotinia sclerotiorum*. J. Nanobiotechnology *19*, 53. https://doi.org/10.1186/s12951-021-00797-5.

5. Kashyap, P.L., Kumar, S., Srivastava, A.K., and Sharma, A.K. (2013). Myconanotechnology in agriculture: a perspective. World J. Microbiol. Biotechnol. *29*, 191–207. https://doi.org/10.1007/s11274-012-1171-6.

6. Yan, X., Pan, Z., Chen, S., Shi, N., Bai, T., Dong, L., Zhou, D., White, J.C., and Zhao, L. (2022). Rice exposure to silver nanoparticles in a life cycle study: effect of dose responses on grain metabolomic profile, yield, and soil bacteria. Environ. Sci, Nano *9*, 2195–2206. https://doi.org/10.1039/d2en00211f.

7. Hamad, A., Khashan, K.S., and Hadi, A. (2020). Silver nanoparticles and silver ions as potential antibacterial agents. J. Inorg. Organomet. Polym. Mater. *30*, 4811–4828. https://doi.org/10.1007/s10904-020-01744-x.

8. El-Naggar, M.A., Alrajhi, A.M., Fouda, M.M., Abdelkareem, E.M., Thabit, T.M., and Bouqellah, N.A. (2018). Effect of silver nanoparticles on toxigenic *Fusarium* spp. and deoxynivalenol secretion in some grains. J. AOAC Int. *101*, 1534–1541. https://doi.org/10.5740/jaoacint.17-0442.

9. Kędziora, A., Speruda, M., Krzyżewska, E., Rybka, J., Łukowiak, A., and Bugla-Płoskońska, G. (2018). Similarities and differences between silver ions and silver in nanoforms as antibacterial agents. Int. J. Mol. Sci. *19*, 444. https://doi.org/10.3390/ijms19020444.

10. Lara, H.H., Romero-Urbina, D.G., Pierce, C., Lopez-Ribot, J.L., Arellano-Jiménez, M.J., and Jose-Yacaman, M. (2015). Effect of silver nanoparticles on *Candida albicans* biofilms: an ultrastructural study. J. Nanobiotechnology *13*, 91. https://doi.org/10.1186/s12951-015-0147-8.

11. Jaidev, L.R., and Narasimha, G. (2010). Fungal mediated biosynthesis of silver nanoparticles, characterization and antimicrobial activity. Colloids Surf. B Biointerfaces *81*, 430–433. https://doi.org/10.1016/j.colsurfb.2010.07.033.

12. Aguilar-Méndez, M.A., San Martín-Martínez, E., Ortega-Arroyo, L., Cobián-Portillo, G., and Sánchez-Espíndola, E. (2011). Synthesis and characterization of silver nanoparticles: effect on phytopathogen *Colletotrichum gloesporioides*. J. Nanopart. Res. *13*, 2525–2532. https://doi.org/10.1007/s11051-010-0145-6.

13. Wani, I.A., Khatoon, S., Ganguly, A., Ahmed, J., Ahmad, T., and Manzoor, N. (2013). Structural characterization and antimicrobial properties of silver nanoparticles prepared by inverse microemulsion method. Colloids Surf. B Biointerfaces *101*, 243–250. https://doi.org/10.1016/j.colsurfb.2012.07.001.

14. Gajbhiye, M., Kesharwani, J., Ingle, A., Gade, A., and Rai, M. (2009). Fungus-mediated synthesis of silver nanoparticles and their activity against pathogenic fungi in combination with fluconazole. Nanomedicine. *5*, 382–386. https://doi.org/10.1016/j.nano.2009.06.005.

15. Pietrzak, K., Twarużek, M., Czyżowska, A., Kosicki, R., and Gutarowska, B. (2015). Influence of silver nanoparticles on metabolism and toxicity of moulds. Acta Biochim. Pol. *62*, 851–857.

16. Tarazona, A., Gómez, J.V., Mateo, E.M., Jiménez, M., and Mateo, F. (2019). Antifungal effect of engineered silver nanoparticles on phytopathogenic and toxigenic *Fusarium* spp. and their impact on mycotoxin accumulation. Int. J. Food Microbiol. *306*, 108259. https://doi.org/10.1016/j.ijfoodmicro.2019.108259.

17. Sun, W., Fan, J., Fang, A., Li, Y., Tariqjaveed, M., Li, D., Hu, D., and Wang, W.-M. (2020). *Ustilaginoidea virens*: insights into an emerging rice pathogen. In Annual Review of Phytopathology, *Vol 58*, J.E. Leach and S.E. Lindow, eds, pp. 363–385. https://doi.org/10.1146/annurev-phyto-010820-012908.

18. Wang, X., Wang, J., Lai, D., Wang, W., Dai, J., Zhou, L., and Liu, Y. (2017). Ustiloxin G, a new cyclopeptide mycotoxin from rice false smut balls. Toxins *9*, 54. https://doi.org/10.3390/toxins9020054.

19. Sun, W., Wang, A., Xu, D., Wang, W., Meng, J., Dai, J., Liu, Y., Lai, D., and Zhou, L. (2017). New ustilaginoidins from rice false smut balls caused by *Villosiclava virens* and their phytotoxic and cytotoxic activities. J. Agric. Food Chem. *65*, 5151–5160. https://doi.org/10.1021/acs.jafc.7b01791.

20. Qiu, J., Lu, F., Wang, H., Xie, J., Wang, C., Liu, Z., Meng, S., Shi, H., Shen, X., and Kou, Y. (2020). A candidate gene for the determination of rice resistant to rice false smut. Mol. Breeding *40*, 105. https://doi.org/10.1007/s11032-020-01186-w.

21. Hiremath, S.S., Bhatia, D., Jain, J., Hunjan, M.S., Kaur, R., Zaidi, N.W., Singh, U.S., Zhou, B., and Lore, J.S. (2021). Identification of potential donors and QTLs for resistance to false smut in a subset of rice diversity panel. Eur. J. Plant Pathol. *159*, 461–470. https://doi.org/10.1007/s10658-020-02172-w.

22. Khan, A.U., Malik, N., Khan, M., Cho, M.H., and Khan, M.M. (2018). Fungi-assisted silver nanoparticle synthesis and their applications. Bioprocess Biosyst. Eng. *41*, 1–20. https://doi.org/10.1007/s00449-017-1846-3.

23. Xue, B., He, D., Gao, S., Wang, D., Yokoyama, K., and Wang, L. (2016). Biosynthesis of silver nanoparticles by the fungus *Arthroderma fulvum* and its antifungal activity against genera of *Candida, Aspergillus* and *Fusarium*. Int. J. Nanomedicine *11*, 1899–1906. https://doi.org/10.2147/ijn.S98339.

24. Tiwari, D.K., Jin, T., and Behari, J. (2011). Dose-dependent in-vivo toxicity assessment of silver nanoparticle in Wistar rats. Toxicol. Mech. Methods *21*, 13–24. https://doi.org/10.3109/15376516.2010.529184.

25. Ali, M., Kim, B., Belfield, K.D., Norman, D., Brennan, M., and Ali, G.S. (2015). Inhibition of phytophthora parasitica and P-capsici by silver nanoparticles synthesized using aqueous extract of *Artemisia absinthium*. Phytopathology *105*, 1183–1190. https://doi.org/10.1094/phyto-01-15-0006-r.

26. Osonga, F.J., Akgul, A., Yazgan, I., Akgul, A., Eshun, G.B., Sakhaee, L., and Sadik, O.A. (2020). Size and shape-dependent antimicrobial activities of silver and gold nanoparticles: a model study as potential fungicides. Molecules *25*, 2682. https://doi.org/10.3390/molecules25112682.

27. Gliga, A.R., Skoglund, S., Wallinder, I.O., Fadeel, B., and Karlsson, H.L. (2014). Size-dependent cytotoxicity of silver nanoparticles in human lung cells: the role of cellular uptake, agglomeration and Ag release. Part. Fibre Toxicol. *11*, 11. https://doi.org/10.1186/1743-8977-11-11.

28. Vyshnava, S.S., Kanderi, D.K., Panjala, S.P., Pandian, K., Bontha, R.R., Goukanapalle, P.K.R., and Banaganapalli, B. (2016). Effect of silver nanoparticles against the formation of biofilm by *Pseudomonas aeruginosa* an in silico approach. Appl. Biochem. Biotechnol. *180*, 426–437. https://doi.org/10.1007/s12010-016-2107-7.

29. Shen, T., Wang, Q., Li, C., Zhou, B., Li, Y., and Liu, Y. (2020). Transcriptome sequencing analysis reveals silver nanoparticles antifungal molecular mechanism of the soil fungi *Fusarium* solani species complex. J. Hazard Mater. *388*, 122063. https://doi.org/10.1016/j.jhazmat.2020.122063.

30. Klionsky, D.J. (2007). Autophagy: from phenomenology to molecular understanding in less than a decade. Nat. Rev. Mol. Cell Biol. *8*, 931–937. https://doi.org/10.1038/nrm2245.

31. Duan, Z., Chen, Y., Huang, W., Shang, Y., Chen, P., and Wang, C. (2013). Linkage of autophagy to fungal development, lipid storage and virulence in *Metarhizium robertsii*. Autophagy *9*, 538–549. https://doi.org/10.4161/auto.23575.

32. Meng, S., Liu, Z., Shi, H., Wu, Z., Qiu, J., Wen, H., Lin, F., Tao, Z., Luo, C., and Kou, Y. (2021). UvKmt6-mediated H3K27 trimethylation is required for development, pathogenicity, and stress response in *Ustilaginoidea virens*. Virulence *12*, 2972–2988. https://doi.org/10.1080/21505594.2021.2008150.

33. Lu, S., Sun, W., Meng, J., Wang, A., Wang, X., Tian, J., Fu, X., Dai, J., Liu, Y., Lai, D., and Zhou, L. (2015). Bioactive bis-naphtho-gamma-pyrones from rice false smut pathogen *Ustilaginoidea virens*. J. Agric. Food Chem. *63*, 3501–3508. https://doi.org/10.1021/acs.jafc.5b00694.

34. Zhao, X., Zhou, L., Riaz Rajoka, M.S., Yan, L., Jiang, C., Shao, D., Zhu, J., Shi, J., Huang, Q., Yang, H., and Jin, M. (2018). Fungal silver nanoparticles: synthesis, application and challenges. Crit. Rev. Biotechnol. *38*, 817–835. https://doi.org/10.1080/07388551.2017.1414141.

35. Sahana, R., Kiruba Daniel, S., Sankar, S.G., Archunan, G., Vennison, S.J., and Sivakumar, M. (2014). Formulation of bactericidal cold cream against clinical pathogens using *Cassia auriculata* flower extract-synthesized Ag nanoparticles. Green Chem. Lett. Rev. *7*, 64–72. https://doi.org/10.1080/17518253.2014.895859.

36. Faghri Zonooz, N., and Salouti, M. (2011). Extracellular biosynthesis of silver nanoparticles using cell filtrate of *Streptomyces* sp ERI-3. Sci. Iran. *18*, 1631–1635. https://doi.org/10.1016/j.scient.2011.11.029.

37. Sun, Y., and Xia, Y. (2002). Shape-controlled synthesis of gold and silver nanoparticles. Science *298*, 2176–2179. https://doi.org/10.1126/science.1077229.

38. Xia, Z.-K., Ma, Q.-H., Li, S.-Y., Zhang, D.-Q., Cong, L., Tian, Y.-L., and Yang, R.-Y. (2016). The antifungal effect of silver nanoparticles on *Trichosporon asahii*. J. Microbiol. Immunol. Infect. *49*, 182–188. https://doi.org/10.1016/j.jmii.2014.04.013.

39. Jian, Y., Chen, X., Ahmed, T., Shang, Q., Zhang, S., Ma, Z., and Yin, Y. (2022). Toxicity and action mechanisms of silver nanoparticles against the mycotoxin-producing fungus *Fusarium graminearum*. J. Adv. Res. *38*, 1–12. https://doi.org/10.1016/j.jare.2021.09.006.

40. Foldbjerg, R., Jiang, X., Miclăuş, T., Chen, C., Autrup, H., and Beer, C. (2015). Silver nanoparticles - wolves in sheep's clothing? Toxicol. Res. *4*, 563–575. https://doi.org/10.1039/c4tx00110a.

41. Lin, J., Shi, S.-S., Zhang, J.-q., Zhang, Y.-j., Zhang, L., Liu, Y., Jin, P.-p., Wei, P.-F., Shi, R.-h., Zhou, W., and Wen, L.-p. (2016). Giant cellular vacuoles induced by rare earth oxide nanoparticles are abnormally enlarged endo/lysosomes and promote mTOR-dependent TFEB nucleus translocation. Small *12*, 5759–5768. https://doi.org/10.1002/smll.201601903.

42. Tong, Y., Feng, A., Hou, X., Zhou, Q., and Hu, X. (2019). Nanoholes regulate the phytotoxicity of single-layer molybdenum disulfide. Environ. Sci. Technol. *53*, 13938–13948. https://doi.org/10.1021/acs.est.9b04198.

43. Park, E.-J., Lee, G.-H., Shim, H.-W., Kim, J.-H., Cho, M.-H., and Kim, D.-W. (2014). Comparison of toxicity of different nanorod-type TiO2 polymorphs in vivo and in vitro. J. Appl. Toxicol. *34*, 357–366. https://doi.org/10.1002/jat.2932.

44. Stern, S.T., and Johnson, D.N. (2008). Role for nanomaterial-autophagy interaction in neurodegenerative disease. Autophagy *4*, 1097–1100. https://doi.org/10.4161/auto.7142.

45. Chen, Y., Yang, L., Feng, C., and Wen, L.P. (2005). Nano neodymium oxide induces massive vacuolization and autophagic cell death in non-small cell lung cancer NCI-H460 cells. Biochem. Biophys. Res. Commun. *337*, 52–60. https://doi.org/10.1016/j.bbrc.2005.09.018.

46. Seleverstov, O., Zabirnyk, O., Zscharnack, M., Bulavina, L., Nowicki, M., Heinrich, J.-M., Yezhelyev, M., Emmrich, F., O'Regan, R., and Bader, A. (2006). Quantum dots for human mesenchymal stem cells labeling. A size-dependent autophagy activation. Nano Lett. *6*, 2826–2832. https://doi.org/10.1021/nl0619711.

47. Kruth, H.S., Jones, N.L., Huang, W., Zhao, B., Ishii, I., Chang, J., Combs, C.A., Malide, D., and Zhang, W.Y. (2005). Macropinocytosis is the endocytic pathway that mediates macrophage foam cell formation with native low density lipoprotein. J. Biol. Chem. *280*, 2352–2360. https://doi.org/10.1074/jbc.M407167200.

48. Wong, B.S.E., Hu, Q., and Baeg, G.H. (2017). Epigenetic modulations in nanoparticle-mediated toxicity. Food Chem. Toxicol. *109*, 746–752. https://doi.org/10.1016/j.fct.2017.07.006.

49. Gedda, M.R., Babele, P.K., Zahra, K., and Madhukar, P. (2019). Epigenetic aspects of engineered nanomaterials: is the collateral damage inevitable? Front. Bioeng. Biotechnol. *7*, 228. https://doi.org/10.3389/fbioe.2019.00228.

50. Mytych, J., Zebrowski, J., Lewinska, A., and Wnuk, M. (2017). Prolonged effects of silver nanoparticles on p53/p21 pathway-mediated

proliferation, DNA damage response, and methylation parameters in HT22 hippocampal neuronal cells. Mol. Neurobiol. *54*, 1285–1300. https://doi.org/10.1007/s12035-016-9688-6.

51. Shyamasundar, S., Ng, C.T., Yung, L.Y.L., Dheen, S.T., and Bay, B.H. (2015). Epigenetic mechanisms in nanomaterial-induced toxicity. Epigenomics *7*, 395–411. https://doi.org/10.2217/epi.15.3.

52. Zhang, T., Du, E., Liu, Y., Cheng, J., Zhang, Z., Xu, Y., Qi, S., and Chen, Y. (2020). Anticancer effects of zinc oxide nanoparticles through altering the methylation status of histone on bladder cancer cells. Int. J. Nanomedicine *15*, 1457–1468. https://doi.org/10.2147/ijn.S228839.

53. Kaundal, B., Kushwaha, A.C., Srivastava, A.K., Karmakar, S., and Choudhury, S.R. (2020). A non-viral nano-delivery system targeting epigenetic methyltransferase EZH2 for precise acute myeloid leukemia therapy. J. Mater. Chem. B *8*, 8658–8670. https://doi.org/10.1039/d0tb01177k.

54. Kotzybik, K., Gräf, V., Kugler, L., Stoll, D.A., Greiner, R., Geisen, R., and Schmidt-Heydt, M. (2016). Influence of different nanomaterials on growth and mycotoxin production of *Penicillium verrucosum*. PLoS One *11*, e0150855. https://doi.org/10.1371/journal.pone.0150855.

STAR★METHODS

KEY RESOURCES TABLE

REAGENT or RESOURCE	SOURCE	IDENTIFIER
Antibodies		
Histone H3K27me3 antibody (pAb)	Active motif	Cat#39155; RRID: AB_2561020
Anti-Histone H3 Mouse Monoclonal Antibody	Huabio	Cat#M1309-1
HRP-labeled Goat Anti-Rabbit IgG (H + L)	Beyotime	Cat#A208
HRP-labeled Goat Anti-Mouse IgG (H + L)	Beyotime	Cat#A216
Chemicals, peptides, and recombinant proteins		
Nano Silver (2 nm)	Aladdin	Cat#N196423
Nano Silver (10–15 nm)	Aladdin	Cat#N196422
FM4-64	Invitrogen	Cat#T13320
Trizol	Sangon Biotech	Cat#B511311
Tris Base	Yeasen	Cat#60102ES80
$MgCl_2$	Sigma-Aldrich	Cat#M2670
KCl	Hushi	Cat#7447-40-7
Sucrose	Hushi	Cat#57-50-1
Glycerol	Coolaber	Cat#CG5811
Glucose	Sigma-Aldrich	Cat#G7021
DTT	Rhawn	Cat#R017350
Protease Inhibitor Cocktail	Roche	Cat#04693116001
Triton X-100	Sigma-Aldrich	Cat#T8787
β-Mercaptoethanol	Macklin	Cat#M828395
Critical commercial assays		
PrimeScript™ RT reagent Kit with gDNA Eraser	TaKaRa	Cat#RR047A
SYBR Green qPCR Master Mix	Yeasen	Cat#11201ES03
Super ECL Detection Reagent ECL	Yeasen	Cat#36208ES60
Deposited data		
Raw and analyzed data	This paper	Accession code: PRJNA889239
Kmt6 RNA seq data	(Meng et al.,2021)[32]	https://doi.org/10.1080/21505594.2021.2008150
Experimental models: Organisms/strains		
TP309 (*Oryza sativa* L. cultivar)	China National Rice Research Institute	N/A
Wanxian 98 (*Oryza sativa* L. cultivar)	China National Rice Research Institute	N/A
HWD	Junbin Huang of Huazhong Agriculture University	N/A
Δ*Uvkmt6*-16, −18 and Δ*Uvkmt6*-C strains	(Meng et al.,2021)[32]	N/A
Oligonucleotides (Primers used in this study, see Table S1)		
Software and algorithms		
ImageJ	N/A	http://rsb.info.nih.gov/
Adobe Illustrator 2020	N/A	https://www.adobe.com/cn/products/illustrator.html

(*Continued on next page*)

Continued

REAGENT or RESOURCE	SOURCE	IDENTIFIER
Microsoft Excel	Microsoft, Richmond USA	https://www.microsoft.com
Cytoscape	N/A	https://cytoscape.org/
TBtools	N/A	https://www.tbtools.com/home

RESOURCE AVAILABILITY

Lead contact

Further information and requests for resources and reagents should be directed to and will be fulfilled by the lead contact, Yanjun Kou (kouyanjun@caas.cn).

Materials availability

This study did not generate new unique reagents.

Data and code availability

- All data reported in this paper will be shared by the lead contact upon request.
- RNA-seq datasets generated in this study have been deposited in the National Center for Biotechnology Information (NCBI) repository under the accession code PRJNA889239.
- Any additional information required to reanalyze the data reported in this paper is available from the lead contact upon request.

EXPERIMENTAL MODEL AND SUBJECT DETAILS

Strains and growth inhibition determination

The *U. virens* strain HWD provided by Prof. Junbin Huang of Huazhong Agriculture University (China) was used as the wild-type in this study. The derived mutants Δ*Uvkmt6*-16, −18 and complemented strain Δ*Uvkmt6*-C were constructed in our previous study.

To calculate the EC_{50} and EC_{90} concentrations (AgNPs concentrations at colony growth inhibition rates of 50 and 90%, respectively) of AgNPs, the wild-type *U. virens* strain was cultured on potato sucrose agar (PSA, 20 g sucrose, 200 g potato, 10 g agar and set the volume with water to 1 L) plates or PSA supplemented with 2 nm or 15 nm AgNPs (Aladdin, N196423 and N196422) under the dark condition at 28°C. The final concentrations of AgNPs were 0.5, 1, 1.5, 2, 2.5, 5 and 10 μg/mL. After 14 days, the colony diameters were measured from two vertical directions to obtain the average colony diameter and calculate the growth inhibition rate. The EC_{50} and EC_{90} concentrations were calculated by fitting a curve using a straight-line model. These tests were repeated twice with three repetitions for each concentration.

To evaluate the effects of AgNPs on the growth and conidiation of *U. virens*, the mycelial plugs were cultured in the liquid potato sucrose (PS) medium with AgNPs at concentrations equal to 0 μg/mL, EC_{50} and EC_{90} for 7 days to determine the mycelial dry weight, the sizes of mycelial pellets and conidial numbers. These tests were repeated twice with three replicates for each concentration.

METHOD DETAILS

Infection assay of *U. virens*

Plugs of *U. virens* strain HWD were cultured in the liquid PS medium for 6 days at 28°C. The mycelia and conidia were crushed and tweaked to 1×10^6 conidia/mL. To determine whether AgNPs affect the virulence of *U. virens*, AgNPs with EC_{50} and EC_{90} concentrations were supplemented when the mixture of hyphae and spores was injected into rice panicles of cultivar TP309 (an *U. virens* susceptible variety, *Oryza sativa* L. cultivar) at the booting stage. After 2 days of darkness, the inoculated plants grew in a greenhouse providing a 14 h photoperiod with a 90% high humidity. The number of rice false smut balls was counted and images were taken at 21 days post inoculation.

Scanning electron microscope (SEM) and transmission electron microscopy (TEM) observations

To observe the morphology of AgNPs used in this study, AgNPs solutions were dried on the cooper mesh and imaged with a TEM (JEM-1010, JEOL, Japan).

To determine the effect of AgNPs on the morphology of *U. virens* cells, HWD plugs were inoculated in the PS medium for 7 days, and then cultured for 5 h after adding AgNPs with EC_{50} and EC_{90} concentrations, respectively. The resultant hyphae were fixed with 2.5% (v/v) glutaraldehyde solution, stained with 1% (w/v) osmium tetroxide and dehydrated with a series of ethanol solutions (30–100%) at room temperature The images of the *U. virens* cells were captured with the SEM (SU8010, Hitachi, Japan) and TEM (H7650, JEOL, Japan).

FM4-64 staining and imaging

To analyze the effect of AgNPs on the cell membranes of *U. virens*, the mycelia plugs were cultured in PS medium for 7 days and treated with AgNPs at the final concentrations of EC_{50} and EC_{90} for 5 h. Then, the mycelia were stained with a membrane-selective red fluorescent dye FM4-64 (7.5 μM, Invitrogen, T13320), which is widely used to study endocytosis and exocytosis, vesicle trafficking and organelle organization, at 28°C for 20 min. After washing the stained sample with water, the images were captured with an Olympus fluorescent microscopy BX53. The images were processed with the software ImageJ from the National Institutes of Health (http://rsb.info.nih.gov/) and organized in Adobe Illustrator.

RNA-seq and bioinformatics analyses

The 7-day cultured mycelia of the wild-type *U. virens* strain HWD in PS media were treated with AgNPs of EC_{50} final concentration for 5 h to collect samples for RNA-seq analysis. Total RNA was extracted using the mirVana miRNA Isolation Kit (Ambion) following the manufacturer's protocol. RNA integrity was evaluated using the Agilent 2100 Bioanalyzer (Agilent Technologies, Santa Clara, CA, USA). The samples with RNA Integrity Number (RIN) $\geq$ 7 were subjected to construct the libraries using TruSeq Stranded mRNA LTSample Prep Kit (Illumina, San Diego, CA, USA) according to the manufacturer's instructions. These libraries were then sequenced on the Illumina sequencing platform (Illumina HiSeq X Ten) to generate 125 bp/150 bp paired-end reads. All experiments were performed with three independent biological replicates.

Raw data (raw reads) from RNA-seq were processed using Trimmomatic to remove the reads containing ploy-N and the low-quality reads and obtain the clean reads. Then the clean reads were mapped to the reference genome using hisat. Fragments per kilobase of exon per million reads mapped (FPKM) value of each gene was calculated using cufflinks, and the read counts of each gene were obtained by htseq-count. Differentially expressed genes (DEGs) were identified using the inoculated for one day functions estimateSizeFactors and nbinomTest, with the threshold p value <0.05 and $|\log2FC| > 1$. The gene ontology (GO) and Kyoto Encyclopedia of gene and Genomes (KEGG) functional enrichment were carried out on the website (https://www.omicshare.com/tools/) and cytoscape. RNA-seq datasets generated in this study have been deposited in the National Center for Biotechnology Information (NCBI) repository under the accession code PRJNA889239.

Quantitative real-time PCR (qRT-PCR) analysis

The mycelia of *U. virens* strain HWD were cultured in the liquid PS medium at 28°C and 180 rpm for 7 days, and then 2 nm AgNPs with a final concentration of EC_{50} were added to the medium for 5 h. AgNPs free medium was used as control. The mycelia were collected to extract total RNA using the Trizol (Sango Biotech, B511311) following the manufacturer's protocol. Reverse-transcription of total RNA was performed with PrimeScript™ RT reagent Kit with gDNA Eraser (TAKARA, RR047A). SYBR Green qPCR Master Mix (Yeason, 11201ES03) was used to conduct the qRT-PCR assay. The $2^{-\Delta\Delta Ct}$ method was used to evaluate the relative expression levels of genes with the *tubulin* gene (*UV8b_900*) as an endogenous reference. The primers used in this study were listed in the Table S1. All experiments were conducted with three independent biological replicates.

Toxicity assays

The mycelia of *U. virens* strain HWD were cultured in the PS medium with AgNPs at final concentrations of EC_{50} and EC_{90} for 7 days. The liquid cultures were filtered with a layer of microcloth. The resultant filtrates

were heat treated and then cultured with the seeds of rice cultivar Wanxian 98 (an *U. virens* susceptible variety, *O. sativa* L. cultivar) to determine the seeds germination. The culture medium without the HWD strain and AgNPs served as control. These experiments were repeated three times with more than 50 seeds each time.

Detection of H3K27me3 via immunoblotting

To detect the level of H3K27me3 modification in the mycelia treated with or without AgNPs, nuclear proteins were extracted. Briefly, 0.2 g of mycelia were ground with liquid nitrogen and suspended in buffer I (20 mM Tris-HCl pH 7.5, 2 mM $MgCl_2$, 20 mM KCl, 250 mM Sucrose, 25% Glycerol, and 50 mM DTT) with 1 × protease inhibitor (Protease Inhibitor Cocktail, Roche, 04693116001). The total protein solutions were centrifuged at 1000 g for 10 min. The resultant supernatants were centrifuged at 10000 g for 20 min at 4°C to pellet nuclei, which were then washed six times with buffer II (20 Mm Tris-HCl pH 7.5, 25 mM $MgCl_2$, 25% glycerol and 0.2% Triton X-100) with 1× protease inhibitor. The washed pellets were re-suspended with buffer I to gain nuclear protein solutions. The nuclear proteins were resolved in a 15% SDS-PAGE gel and transferred to the PVDF membrane, which was incubated with primary antibody anti-H3K27me3 antibody (Active motif, 39155), anti-Histone 3 antibody (Huabio, M1309-1) and HRP-conjugated secondary antibody (Beyotime, A0208 and A0216). The blots were imaged with a chemiluminescence kit (Super ECL Detection Reagent ECL, Yeasen, 36208ES60) by a Yeasen imaging system.

QUANTIFICATION AND STATISTICAL ANALYSIS

Quantification and statistical analysis were performed using Microsoft Excel for mycelial dry weight, conidial concentration, number of smut balls, relative expression of genes, rice shoot length and inhibition rate data. At least three biological replicates were performed for each experiment. Data are given as the means ± SD. Pairwise Student's t-tests and two-tailed ANOVA were used to quantify statistically significant difference between datasets. p values were regarded as significantly different at $p < 0.05$.